

Sox9-related signaling controls zebrafish juvenile ovary–testis transformation

D Sun^{1,5}, Y Zhang^{1,5}, C Wang¹, X Hua², XA Zhang³ and J Yan^{*,1,4}

In almost all vertebrates, the downstream of the *sox9* signaling axis is well conserved for testis differentiation. The upstream genes of this pathway vary from species to species during evolution. Yet, little is known about how these signaling cascades are regulated and what cellular processes are dominant in ovary–testis transformation in juvenile zebrafish. In this study, we find that the transforming gonads undergo activation of *sox9a*-expressing stromal cells with increased deposition of extracellular matrix and formation of degenerative compartments. This leads to follicle disassembly, oocyte degeneration, follicle cell-*cyp19a1a-amh* conversions, and, eventually, formation of the testis cord. *In vitro* primary culture of juvenile ovary tissue in gonadotropins increases cytoplasmic accumulation of *sox9a* and p-Erk1/2, and induces mesenchymal morphology. MAPK inhibitors (MKI), a mixture of PD98059 and U0216, eliminate the cytoplasmic distribution but do not eradicate nuclear localization of *sox9a* and p-Erk1/2. Nuclear p53 are relatively increased in MKI-treated cells that exhibit less spreading and reduced proliferation. Despite uniform nuclear condensation, only a fraction of cells displayed the apoptotic phenotype. These results suggest that high levels of cytoplasmic *sox9a* and p-Erk1/2 activity activate stromal cells and enhance the production of extracellular matrix required for testis cord formation, whereas deregulation and translocation of *sox9a* and p-Erk1/2 induce follicle disassembly and incomplete apoptosis associated with nuclear p53. Together with the established FSH/cAMP/MAPK/AMH pathway in mammalian granulosa and Sertoli cells, we demonstrated that the *sox9* axis signaling that determines testis formation in mammals also induces zebrafish ovary–testis transition, and adds to its conserved role in sex reversal.

Cell Death and Disease (2013) 4, e930; doi:10.1038/cddis.2013.456; published online 21 November 2013

Subject Category: Experimental Medicine

In mammals, gonad development can be divided into two phases: formation of the indifferent genital ridge/bipotential gonad and sex differentiation.¹ The indifferent gonads are initially developed from the mesothelial layer of the peritoneum. As embryos grow, some cells of mesonephric origin join the gonad ridge and form the primary sex cord. Thus, the early gonad is an undifferentiated primordium composed of bipotential somatic stem cells that are precursors for supporting cells and steroid-secreting cells. Primordial germ cells (PGCs) arise from the dorsal endoderm of the yolk sac near the allantois, migrate along the hindgut and dorsal mesentery, and eventually join the gonadal ridge.²

When the PGCs reach the gonadal ridge, the supporting cell precursors become either testis-specific Sertoli cells or ovary-specific follicle (granulosa) cells. Meanwhile, the immigrating mesonephric cells give rise to peritubular myoid (PM) cells (endothelial cells that form the male-specific vasculature) and fetal steroidogenic-Leydig cells (ovarian

theca cells).^{1,3} Parallel to somatic precursors, PGCs differentiate into oogonia in ovarian follicles or spermatogonia in Sertoli cells dominant testis cord.

Compared with mammals, fishes exhibit a striking plasticity in the sex determination process, and show a wide range of gonad differentiation mechanisms, such as hermaphroditism and gonochorism.⁴ Hermaphrodite fishes can have either functional male and female gonadal tissues simultaneously (synchronous) or sequentially change their sex (sequential) from male to female or from female to male. In differentiated gonochoristic species, an indifferent gonad directly differentiates into a testis or an ovary. Zebrafish are undifferentiated gonochoristic fishes: during the juvenile period,⁵ all individuals develop undifferentiated ovary-like gonads containing immature oocytes.⁶ Between 20 and 30 days post fertilization (d.p.f.), immature oocytes develop into ovaries in approximately half of the zebrafish population. In the remaining population, the immature oocytes degenerate and the gonads

¹Department of Biology, Institute for Marine Biosystems and Neurosciences, Shanghai Ocean University, Shanghai, 201306, China; ²Department of Cancer Biology, Abramson Family Cancer Research Institute, University of Pennsylvania, Philadelphia, PA 19104, USA; ³Stephenson Cancer Center and Department of Physiology, The University of Oklahoma Health Sciences Center, Oklahoma City, OK 73104, USA and ⁴Key Laboratory of Exploration and Utilization of Aquatic Genetic Resources, Shanghai Ocean University, Ministry of Education, Shanghai, China

*Corresponding author: J Yan, Shanghai Ocean University, 999 Hucheng Huan Road, Shanghai 201306, China. Tel: +86 21 61900488; Fax: +86 21 61900455; E-mail: jyan2@shou.edu.cn

⁵These authors contributed equally to this work.

Keywords: zebrafish; sex reversal; incomplete apoptosis; MAPK pathway; *sox9*

Abbreviations: MKI, MAPK (mitogen-activated protein kinase) inhibitor; p-Erk1/2, phosphorylated Erk1/2; p-Mek1/2, phosphorylated Mek1/2; HCG, human chorionic gonadotropin; FSH, follicle-stimulating hormone; PGC, primordial germ cell; d.p.f., days post fertilization; Gc, gonocytes; Cn, nucleus-condensed cells; PO, perinucleolar oocyte; Tc, testicular cord; Sc, spermatogonia cysts; Mn, multinucleated giant cell; Dc, degenerative compartment; GTCM, basic gonadal tissue culture medium; EMT, epithelial–mesenchymal transition; ECM, extracellular matrix; HE, hematoxylin and eosin; TUNEL, terminal dUTP nick end-labeling

Received 17.9.13; revised 19.10.13; accepted 21.10.13; Edited by A Stephanou

acquire testis morphology. Therefore, the zebrafish is an optimal model with which to investigate cell death and differentiation for sex reversal. Direct evidence for plasticity of germline stem cells comes from spermatogonial stem cell transplantation in zebrafish. Spermatogonial stem cells are able to colonize in the recipient ovaries and differentiate into female germ line cells.⁷

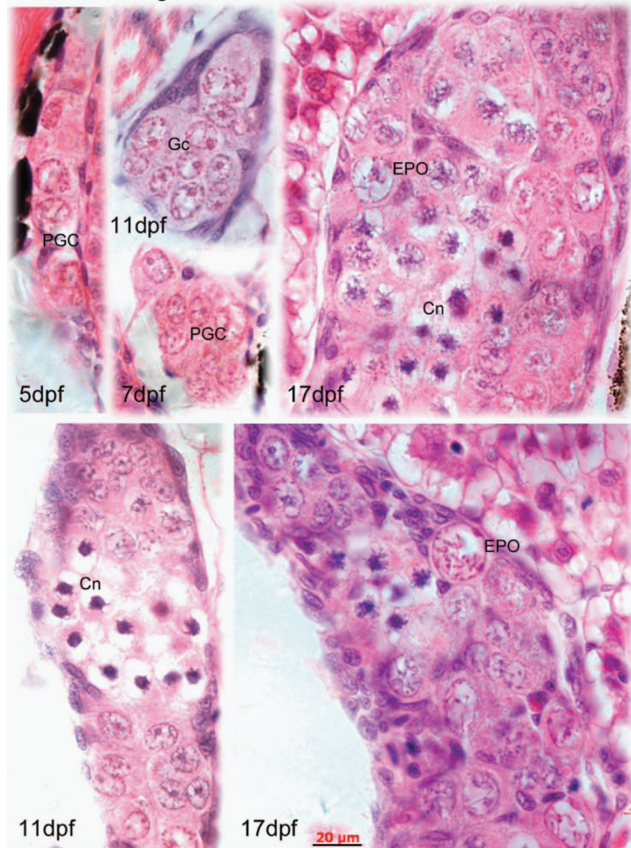
Two cellular mechanisms for sex reversal have been proposed: apoptosis and transdifferentiation. The apoptosis mechanism stipulates that a large amount of oocyte apoptosis results in a weakened oocyte-derived signal and reduced aromatase expression. Consequently, in this model, testosterone is not converted to estrogen, spermatogenesis ensues, and the gonad becomes a testis. According to the transdifferentiation mechanism, follicular cells in oocyte-depleted follicles survive, proliferate, and transdifferentiate into Sertoli cells.⁸ There is still no direct evidence to link oocyte apoptosis to cell transformation in juvenile zebrafish gonads. Much remains to be learned about the signals activating juvenile oocyte degeneration, and the extent to which the signals involved in ovary apoptosis also contribute to ovary–testis transition.

Results

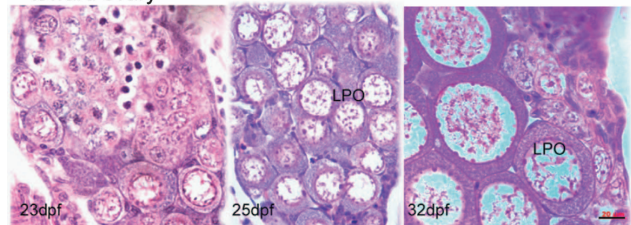
Time course of gonadogenesis. Gonadal development and sex differentiation were examined histologically. A minimum of six fish were sampled every 5 days, starting at 5 d.p.f. and continuing until 55 d.p.f. Serial sections were prepared to determine the developmental stage of the gonads (Figure 1 and Supplementary Figure 1). At 5 d.p.f., we observed PGCs clustered in groups of 3–5 cells (Figure 1a). Flattened and basophilic somatic cells surrounded the PGC clusters (Figure 1a). By 11 d.p.f., the number of germ cells increased, and some PGCs began to differentiate into gonocytes (Gc) that possess rather homogeneous, slightly basophilic karyoplasm, and contain one or more nucleoli in the large nucleus (Figure 1a). Almost at the same time, nucleus-condensed cells (Cn), Gc containing a nucleus with condensed chromatin, appeared. The morphological characteristics of Cn were recognized as entry into meiosis. At this stage, the gonads containing both Gc and Cn were categorized as indifferent gonads, because male- and female-specific Gc of fishes are difficult to differentiate solely based on cell morphological characteristics.

Sex differentiation began as early as 17 d.p.f., as indicated by the appearance of perinucleolar oocytes (POs; Figure 1a). As the gonads grew into juvenile ovaries from 20 to 25 d.p.f., the number and size of POs increased and somatic cells were located mainly at the gonadal periphery. By quantifying the number of both germ and somatic cells in the gonads, we found that the ratio of meiotic Gc and POs to total gonadal cells was significantly different, such that individual fishes could be divided into two sex populations. At 20 d.p.f., the majority of the cells in the ‘presumptive ovary’ group were meiotic germ cells that became condensed POs at 40 d.p.f. (Figure 1b and Supplementary Figure 1g). The early gonads showed normal (i.e., nontransforming) ovaries and progressed into maturation (Supplementary Figure 1j and 1). Asynchronous cell growth and delayed germ cell differentiation

a indifferent gonads



b toward ovary



c toward testis

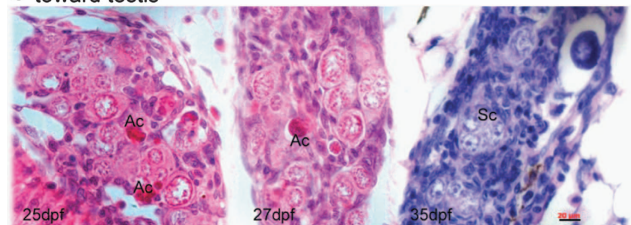


Figure 1 Gonadal development and differentiation. Indifferent gonad (a), only primordial germ cells (PGCs) are found in the gonad at 5 d.p.f. PGCs contain a large nucleus and possess a distinct nuclear membrane, several big nucleoli, and a network of fine chromatin filaments distributed throughout the karyoplasm. Along the inner side of the nuclear membrane, deeply staining granulosa material is seen. The weakly stained cytoplasm accounts for only a small fraction of the cell volume. At 7 d.p.f., PGCs differentiate into gonocytes (Gc). At 11 d.p.f., more Gcs and meiotic gonocytes with condensed chromatin (Cn) are seen, in addition to PGCs. At 17 d.p.f., early perinucleolar oocytes (EPOs) appear. During juvenile gonadal differentiation toward the ovary (b), more meiotic germ cells are seen (23 d.p.f.), showing densely packed oocytes (27 d.p.f.) and tight connections between late perinucleolar oocytes (LPOs) at 32 d.p.f. In the presumptive testis (c), stromal cells increase and oocyte degenerations appear as acid staining cells (Ac). Sc, spermatogonia cyst. Scale bar = 20 µm

occurred in the 'presumptive testis' group: fewer POs and more proliferating somatic cells were observed (Figure 1c and Supplementary Figure 1c and e). From 25 to 55 d.p.f., the gonads underwent ovary-to-testis transformation and testicular cord (Tc) morphogenesis (Supplementary Figure 1h and i). Although the time course of gonadal development (Figure 2) was generally consistent with previous descriptions,⁶ our histological analysis revealed biased sex differentiation toward either the presumptive testis or ovary at the very beginning of juvenile gonadal development.

Cellular conversions from ovarian follicles to testis cords. In contrast to the nontransforming gonads, in which POs progress through meiosis and maturation, the transforming gonads showed activation of somatic stem cells (Figure 1c). The activated stromal cells and increased extracellular matrix (ECM) infiltrated the ovarian cavity and encapsulated the meiotic Gc (Figure 1c), accompanied by the development of spermatogonia cysts (Sc) and the degeneration of oocytes. Oocyte degeneration was evidenced by the appearance of red staining acidic body (presumably apoptotic body) and vacuolated oocytes (Figure 1c). The degenerating oocytes were surrounded by the increased gonadal matrix and mesenchymalized stromal cells and formed a degenerative structure, termed degenerative compartment hereafter (Figure 3a).

Within the degenerative compartments, several cellular changes were observed. First, the follicle cells lost their tight junctions with adjacent cells and detached from the encapsulated oocyte, implying a preparation for eccentric migration and epithelial–mesenchymal transition (EMT) (Figures 3c and d). This extrapolation was based on the fact that granulosa cells are epithelial cells, and morphologically distinct from the stromal cells of mesenchymal origin.⁸ Second, the dissociated oocytes displayed apoptotic morphology with condensation of chromatin and a marked vacuolation. However, nuclear fragmentation and apoptotic bodies were not frequently observed (Figures 3a–e). There were no signs of phagocytosis from neighboring somatic cells, although a few lysosome-like structures with red coloration were seen (Figures 3b and e). Third, many cells retained intact morphology although the disassembled follicles exhibited various degrees of degeneration and decomposition (Figures 3a and c). In the vicinity of the degenerating oocytes, there were proliferating stromal cells, Sc, and a multinucleated giant cell (Mn), displaying gross morphological characteristics of Tc (Figures 3d and e). As degenerating oocytes and newly regenerating testis tissues coexisted in the transforming gonads, it was unclear whether the testis tissues were transformed from the degenerative follicles or regenerated from the reserved stem cells.

Molecular characterization of cellular changes throughout gonadal transition. To characterize the cellular phenotypes within the transforming gonads, we used *sox9a*, *amh*, and *cyp19a1a* to identify Sertoli and granulosa cells, and *vasa* to mark live germ stem cells. Relative to high expression of *vasa* in the nontransforming gonads (Figure 4a), the expression of *vasa* in the transforming gonads displayed weak and circular dot patterns in POs (Figure 4c). As previously

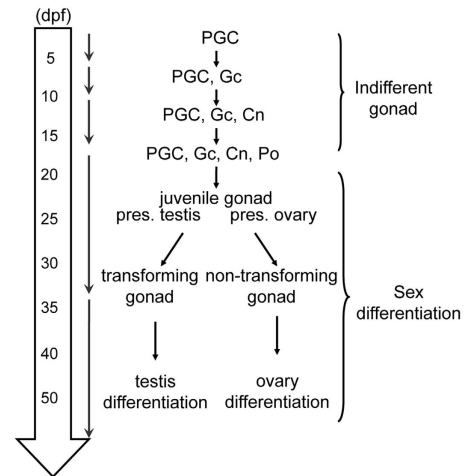


Figure 2 Time course of gonadal development. Before 17 d.p.f., the gonad is indifferent and contains PGCs, Gc, Cn, and perinucleolar oocytes (POs). The gonad commits into sex differentiation at 17 d.p.f. and becomes mature at 35 d.p.f. The interval between 17 and 35 d.p.f. is referred to as the juvenile period, in which the gonad is identified as presumptive ovary or presumptive testis. The presumptive testis must undergo an ovary–testis transition before maturation

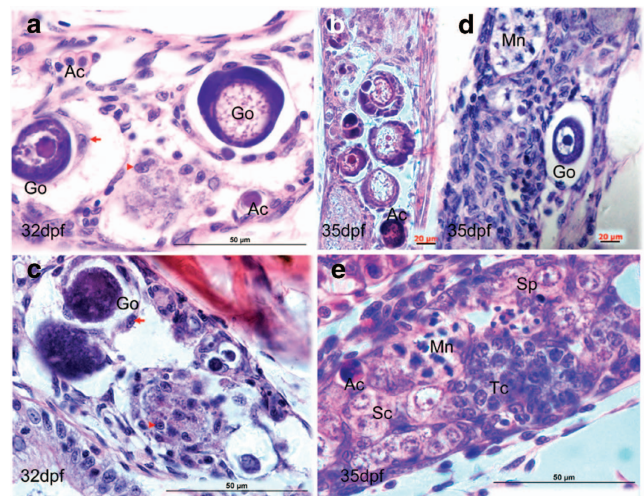


Figure 3 Morphological alterations from ovarian follicle to testis cord. (a) Active stromal cells surround the giant oocytes (Go) and form degenerative compartment (a). Within the degenerative compartment, follicle cells dissociate from the oocytes (b) and acquire mesenchymal morphology (arrow, a). (c) Degeneration of perinucleolar oocytes (primordial follicles) with marked vacuolation and survival cells from the oocyte decomposition (arrowhead). (d) Coexistence of oocyte degeneration and multinucleated giant cells (Mn) that present many peripheral nuclei and annular chromatin. (e) Regeneration of testis cord tissues. Ac, acidic cells with red coloration; Sc, spermatogenic cysts; Sp, spermatogonia; Tc, testis cord-like structure. Scale bars = 20 μm (b, and d) and 50 μm (a, c and e)

reported in the *vasa::egfp* transgenic line,⁹ transforming gonads showed increased expression of *sox9a* and *amh* and decreased expression of *cyp19a1a* and *vasa*, compared with the nontransforming gonads (Figures 4a–d). To further understand the relationship between *amh*-expressing cells and *cyp19a1a*-expressing cells within the transforming gonads, we compared the expression of *cyp19a1a* and

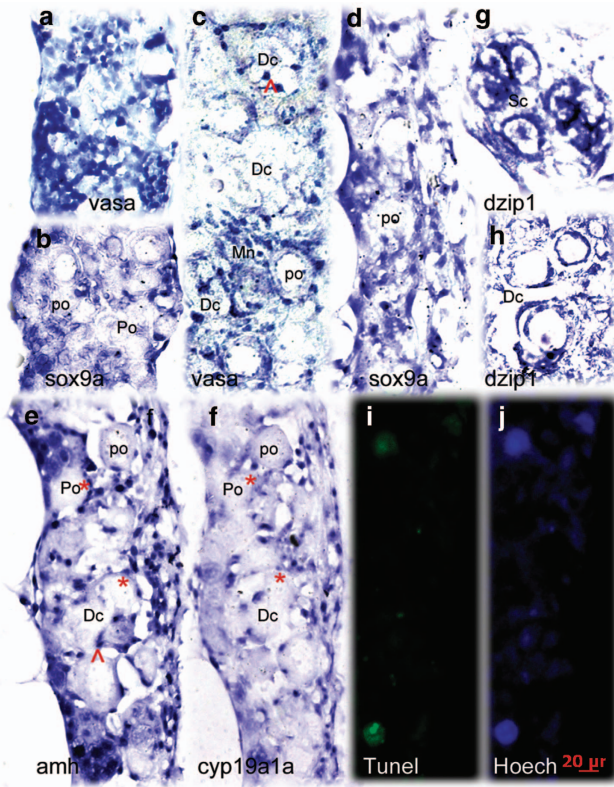


Figure 4 Comparative analysis of the expression pattern of multiple sex determinant genes between transforming and nontransforming gonads at 35 d.p.f. In the nontransforming gonads, *vasa* (a) was highly expressed whereas *sox9a* (b) expression was restricted in the two sides of the gonadal somatic cells. The transforming gonads revealed distinct expression patterns for *vasa* (c), *sox9a* (d), *amh* (e), *cyp19a1a* (f), and *dzip1* (g and h). *amh*, *cyp19a1a*, and *sox9a* were expressed in somatic cells (supporting cells) located in the gonadal matrix and surrounding the oocytes. *dzip1* was highly expressed in both spermatogonia and supporting cells. (e and f) Two adjacent sections with low levels of *cyp19a1a* and high levels of *amh* expressed with partial overlap in the same follicles (asterisk). Abnormally expressing aggregates in degenerative compartment (Dc) are indicated by the arrow. TUNEL staining assay showed the larger TUNEL-positive cells were consistent with degenerative oocytes (i). Hoechst staining (j) was used to count total number of gonadal cells. Go, giant oocyte; Mn, multinucleated giant cells; PO, perinucleolar oocyte. Scale bars = 20 μ m

amh in adjacent sections of the same transforming gonads. It was frequently observed that both markers were coexpressed in the same ovarian follicle. Although *cyp19a1a* expression was downregulated, *amh* expression became increased (Figures 4e and f). Thus, ovary–testis transition was evidenced by switching *cyp19a1a*-expressing cells to *amh*-expressing cells.

Cell transdifferentiation during follicle ovarian–testis transition. As other studies of cellular plasticity have suggested, the ability of follicular cells to switch to their testis counterparts may reflect the similar embryonic origin of these two cell types.⁸ There is evidence that pre-Sertoli cells, Sertoli cells, and granulosa cells share a common precursor in mice.^{10–11} To test this possibility in zebrafish, we selected 19 genes associated with sex-differentiation and examined their expression pattern during gonad development

(Supplementary Tables 1–3). In comparison, the transcript levels of *amh* and *dzip1* were relatively higher in the testis, whereas the expressions of *pou5f1*, *nanos3*, *dazap2*, *na5a2*, *nr5a1b*, and *cyp19a1a* were predominant in the ovary.

We then analyzed the location of RNA expression in testis and ovary. In contrast to *amh* and *cyp19a1a* for which sexually dimorphic expression patterns are confined to somatic cells (Supplementary Figure 3a), *dzip1* and *nanos3* were expressed in both gonadal somatic cells and germ cells. Using *vasa* expression as a control, *nanos3* was predominantly expressed in the oocyte proper as well as the granulosa cells, but also expressed specifically by germ cells at varying stages of spermatogenesis (Supplementary Figure 3b). *Dzip1* colocalized with *dazl* in oocytes and granulosa cells in the follicles, but was predominantly expressed in testis cord-localized premeiotic spermatogonia (Supplementary Figure 3c). Based on their expression bias in both testis and ovary, and known stem cell-association properties,¹² we consider *dzip1* and *nanos3* to be the common markers of germ cells and supporting cells that preferentially develop into testis and ovary.

We then extended our analysis retrospectively to determine whether these genes are expressed in earlier developing embryos. As expected, *vasa*-expressing cells migrated and resided in the presumptive gonads. *Pou5f1*, *nanos3*, and *dzip1* were highly expressed in developing tissues (Supplementary Figure 3d). In the juvenile transforming gonads, *dzip1* was strongly expressed in the Sc and the surrounding supporting cells (Figure 4g), even in the degenerative compartment (Dc) (Figure 4h). *Nanos3* expression was detected in the degenerated oocyte (data not shown). The upregulation of *dzip1*, a stem cell-associated marker, in the supporting cells of the degenerating follicles implies that the follicle cell transition from *cyp19a1a* to *amh* may go through the transdifferentiation process.

Sox9 expression precedes oocyte apoptosis and degeneration. We defined ‘stromal cell activation’ as the combinatory effect of cell proliferation (such as increase in the number of stromal cells), and migration with mesenchymal morphology. Having determined that stromal cell activation was the first step in initiating ovary–testis transformation, we then compared the activation of stromal cells with the expression of *sox9a*. In the transforming gonads, *sox9a*-expressing cells were no longer restricted to the gonadal periphery, but infiltrated into the interior gonadal stroma and surrounded the oocytes. Unlike the dot expression pattern of *vasa*, *amh*, and *cyp19a1a*, *sox9a*-expression showed increased cytoplasmic distribution with mesenchymal morphology (Figure 4d). As the *sox9*-expressing cells and the active stromal cells showed similar mesenchymal morphology and topographic distribution in the transforming gonads (Figure 3c vs 4d), we conclude that *sox9a*-expressing stromal cells or pre-Sertoli cells were first activated to trigger ovary–testis transformation.

To determine whether and to what degree the degenerating follicles undergo apoptosis, we examined and quantified the degeneration of gonadal cells from 20 to 35 d.p.f. using the terminal dUTP nick end-labeling (TUNEL) method

(Supplementary Figure 2 and Figures 4i and j). Of all DAPI staining gonadal cells, ~10% were TUNEL-positive cells in the presumptive male group by 32 d.p.f., whereas only a small proportion of TUNEL-positive cells contained the typical apoptotic bodies (Supplementary Figure 2). TUNEL-positive somatic cells were observed. Although TUNEL-positive cells were more numerous than the morphologically degenerative oocytes, many degenerative follicles were TUNEL negative. We also saw substantial nuclear staining with irregular shapes of *vasa* expression (Figure 4c) and *amh* expression within Dc (Figure 4e). This abnormal staining shape with a high level of *vasa*- and *amh*-RNA expression was in accordance with the histological observations that many cells survived the degeneration. This finding further suggests that many cells are at the pre-apoptotic stage, a transient state of cell morphology for subsequent cell transformation or complete apoptosis. Thereafter, we referred to this as partial apoptosis and referred to partial cellular transformation as incomplete apoptosis. Immunohistochemical analysis revealed that weak expressions of Mek1/2, phosphorylated Mek1/2 (p-Mek1/2), *sox9a*, and p53 were widely detected. Only a fraction of oocytes and the surrounding follicle cells (presumably transforming follicles) showed an increase of staining intensity (Supplementary Figure 4). These results suggest a functional link between p53 and MAPK components and *sox9a*-*amh*/*cyp19a1a* pathways during gonadal transitions from protogenic ovary to early testis.

Sox9 pathways induced mesenchymal morphology changes in primary culture of gonadal tissues. Although histomorphological and histo-*in situ* hybridization analyses indicated that degeneration and transformation were likely induced by MAPK-*sox9a*/p53 pathways, it is still unclear how these pathways are regulated during the juvenile ovary–testis transformation. To this end, we used a mammalian growth factor, human chorionic gonadotropin (HCG), to mimic follicle-stimulating hormone (FSH) activity, and cultured the gonad tissues in the modified culture system. Rather than performing *in vitro* culture of entire gonad,¹³ we sliced the gonad tissue into small pieces. On the fourth day, a monolayer of adherent fibroblast-like cells grew from the periphery of the primary explants. We then added activator-cAMP and/or MKI (MAPK (mitogen-activated protein kinase) inhibitor) and continued the culture for 48 h. Gonadotropin and cAMP induced mesenchymal morphology, cell spreading, and proliferation of the cultured primary cells. In contrast, MKI inhibited proliferation and cell spreading, and repressed *sox9a* and *amh* transcriptions (Supplementary Figure 5, data not shown). These results were consistent with the *in vivo* histological observations that the *sox9a* axis pathways increase ECM production and mesenchymal morphological transformation of gonadal cells.

We next examined how the *sox9a* pathways linked oocyte apoptosis to cellular transformation. Without MKI treatment, the cultured cells exhibited mesenchymal morphology with

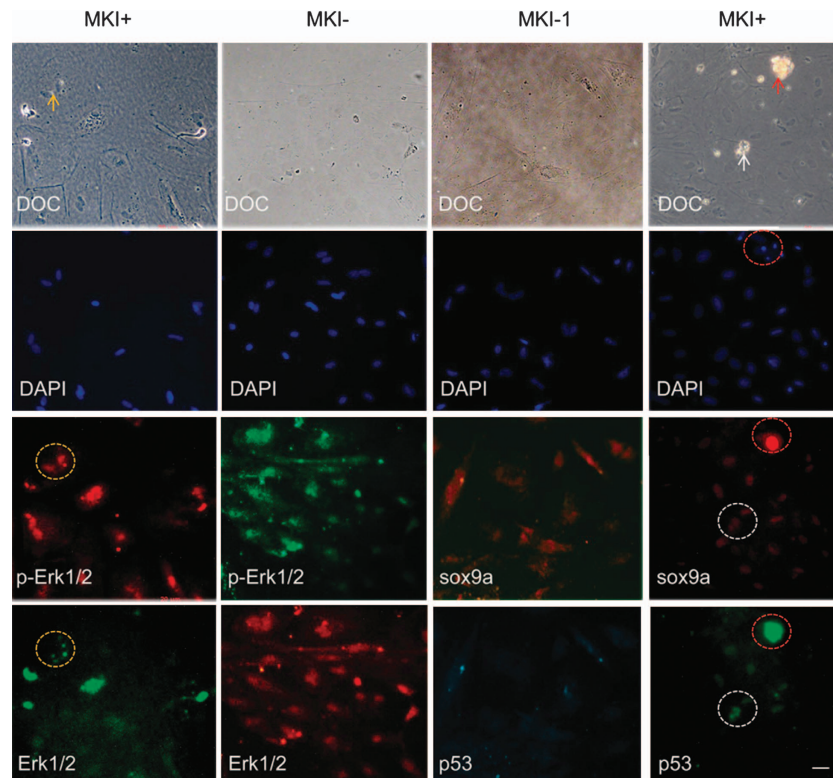


Figure 5 Involvement of MAPK-*sox9a* and p53 pathways in morphological alterations of cultured gonadal tissue. Ovary tissues were sliced and cultured *in vitro*. After 2–3 days, MKI or DMSO control were added and tissues were incubated for 48 h. The cultures were costained with Erk1/2 and p-Erk1/2 antibodies (left two columns) or costained with *sox9a* and p53 antibodies (right two columns). DAPI staining and DOC were seen. Apoptotic or degenerating cells (arrow) and related signal staining (dotted circle) are shown. Scale bars = 20 μ m

abundant extracellular matrix. Sox9a and phosphorylated Erk1/2 (p-Erk1/2) were highly expressed in the cytoplasm. Similar phenotypes were observed in *sox9*-activated stromal cells of the transforming gonads (Figures 3a and 4d). After MKI treatment, levels of *sox9a* and p-Erk1/2 were dramatically decreased in the cytoplasm, whereas nuclear *sox9a* and p-Erk1/2 showed little reduction. In contrast, levels of p53 increased in the nuclei, and cell number decreased. Deregulation and translocation of Erk1/2, p-Erk1/2, *sox9a*, and p53 were indicated by changes of signal intensity (mean values) and size measurement (pixel values) of immunostaining images (Figure 5 and Table 1). The MKI-treated cells became uniformly round with nuclear condensation, and partially apoptotic with fragmented nuclei (Figure 5). These results suggest that cytoplasmic p-Erk1/2 and *sox9a* activate stromal cells and promote ECM production, whereas reduced p-Erk1/2 activity deregulate expression and translocation of *sox9a* and p53, and induce partial apoptosis and cellular transformation (Figure 6).

Discussion

In juvenile zebrafish, the gonadal transition from ovary-like tissue to testis is reminiscent of the sex-specific timing of meiosis entry in mammals. Female PGCs (oogonia) first enter meiosis at birth and undergo oogenesis during juvenile development. In contrast, male PGCs (spermatogonia) do not enter meiosis and spermatogenesis until puberty. It has been proposed that germ stem cells are driven to enter meiosis by an intrinsic clock. Signals produced by the male-specific somatic cells inhibit Gc from entering meiosis, arresting Gc in G1/G0 and directing them toward spermatogenesis. Like many other species, zebrafish do not have obvious sexually dimorphic chromosomes; instead, multiple sex determination loci^{14–16} have been identified to be responsible for sex-associated effects. This study presents compelling evidence that *sox9a* axis pathways orchestrate the supporting cell-dominated transition from ovary to testis.

In the testes, *sox9a* is an upstream positive regulator of *amh* that, in turn, is an upstream negative regulator of *cyp19a1a*.¹⁷ In the ovary, AMH inhibits primordial follicle assembly.¹³ Although the regulatory interactions of *sox9a-amh/cyp19a1a* have been extensively investigated, it is unclear whether and how this pathway is regulated to implement the juvenile ovary–testis transformation in

zebrafish. The present study showed that upregulation of *sox9a* activated stromal cells, increased extracellular matrix production, proceeded follicle cell-*cyp19a1a-amh* conversions, and induced ovarian follicle degeneration and testis cord generation. This somatic cell-dominated sex differentiation model expands the previous hypothesis that ovarian fate is passively determined by a threshold number of developing oocytes,¹⁸ that is, a number of oocytes exceeding the threshold activate the female pathway, whereas a number of oocytes under the threshold induce the male pathway.¹⁸ The loss of female germ cells, by either injecting *dnd* antisense morpholino or mutating *sox9b*,¹⁹ induces female-to-male sex reversal. Loss of germ cells is not an adequate mechanism to explain zebrafish juvenile ovary–testis transition, however. We demonstrated that this transition is regulated by FSH/cAMP/MAPK-*sox9* pathway.

In humans and mice, FSH induces upregulation of AMH expression in Sertoli cells and granulosa cells via its second messenger cAMP.^{20–21} FSH induces an adenylyl cyclase-dependent increase in cAMP levels that activate several kinases in the PKA, PI3K/PKB, p38 MAPK, and MEK1/2-ERK1/2 pathways.^{9,13,20} Here, we propose a novel mechanism to explain how the degenerative oocytes undergo incomplete apoptosis and transform into testis cords during juvenile ovary–testis transition (Figure 6). According to this model, juvenile FSH upregulates *sox9a* expression and distribution in presumptive testis stromal cells via Mek1/2-Erk1/2 pathways. Cytoplasmic *sox9a* activates stromal cells

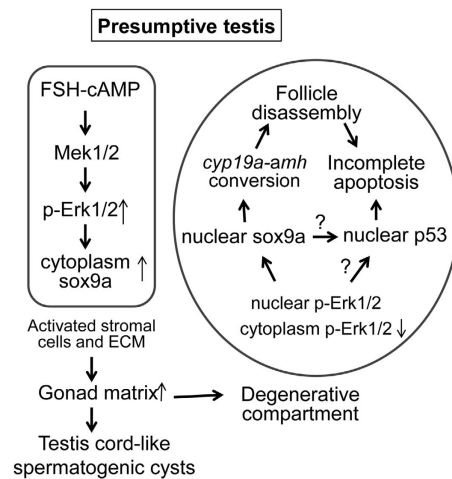


Figure 6 A proposed model that FSH-MAPK-*sox9a*/p53 signaling pathways regulate juvenile ovary–testis transition in zebrafish. In the stromal cells of the presumptive testis group, juvenile FSH upregulates *sox9a* expression and cytoplasmic distribution through phosphorylation of Mek1/2–Erk1/2 signaling. Activated stromal cells and increased ECM form gonad matrix that grows as testis cord-like spermatogenic cysts or becomes degenerative compartments that surround the ovarian follicles. Within the degenerative compartments, p-Erk1/2 and *sox9a* are reduced, particularly in cytoplasm whereas *sox9a* and p53 in nucleus are relatively increased. Misexpression and translocation of *sox9a* deregulates the expression of *amh/cyp19a1a* and induces the follicle disassembly. Meanwhile, nuclear p53 promotes degeneration of the disassociated follicle cells, leading to incomplete apoptosis. Finally, these incompletely apoptotic cells are either transformed to testis cord or die. It is uncertain how p53 is regulated by *sox9a* and p-Erk1/2 are interplayed in the transforming gonads

Table 1 Quantitative analysis of immunostaining signals in Figure 5

Antibody	Parameter	MKI –	MKI +	t-test
p-Erk1/2	Mean	42.3 ± 2.0 ^a	23.1 ± 4.2	<0.001 ^b
	Pixels	2858.6 ± 954.9	1803 ± 496.6	0.06
Erk1/2	Mean	22.8 ± 5.9	15.7 ± 4.8	0.07
	Pixels	2404.2 ± 1463.0	1681.2 ± 659.1	0.343
<i>sox9a</i>	Mean	7.4 ± 1.1	12.4 ± 1.9	0.001
	Pixels	2754.6 ± 1292.1	558.4 ± 145.5	0.019
p53	Mean	9.6 ± 3.5	25.4 ± 4.1	<0.001
	Pixels	2345.4 ± 550.6	713.6 ± 241.0	<0.001

^aAverage values ± S.D.

^bP-values

to form degenerative compartments that surround the ovarian follicles. Because of a blocked blood supply, or other unknown factors within the degenerative compartments, Erk1/2 activity and cytoplasmic sox9a are dramatically reduced with relative increases of nuclear sox9a and p53. Deregulated expression of sox9a and p53 coordinately induce follicle disassembly, apoptotic processes, and cellular transformations.

Germ cell development is unique in that the cells progress through meiosis and break double-strand DNA for homologous recombination. Therefore, maintenance of genome stability in germ cells is required for normal gonad development.^{18,22} Tp53 (p53) has been reported to mediate germ cell apoptosis and regulate oocyte survival through meiosis.^{18,22} On this basis, we theorized that preapoptotic cells might undergo DNA repair through meiotic homologous recombination or mitotic recombination. The recombination provides an opportunity for cells to undergo either transformation or apoptosis. As meiosis is a 'one-way' process for germ cell division and cannot engage in a cell cycle as mitosis does, oocyte degeneration and programmed cell death are regarded as their final fate.

In summary, gene expression analyses in zebrafish have already revealed the conservation of structure, function, and expression of a large number of mammalian genes at the downstream of the sex determination pathway, including *cyp19a1a*, *sox9a*, and *amh*.^{9,13,20} Our results support the idea that *sox9* is a fundamental testis-differentiating gene common to all vertebrates.^{23–24} We demonstrated that *sox9a* expression pattern closely correlates with the behavior of the stromal cells in gonadal tissue of juvenile zebrafish. High level of cytoplasmic *sox9a* expression promotes cellular proliferation, mesenchymal transformation, and ECM deposition, whereas misexpression of *sox9a* induces p53-associated follicle degeneration and cell transformation. Obviously, the expression and nuclear translocation of *sox9a* and p53 are regulated by Mek1/2–Erk1/2 MAPK signaling. The exact regulatory mechanisms in MAPK–*sox9*/p53 pathway remain for further investigations. Therefore, the manipulation of sex determination might be possible via indirectly disrupting upstream regulatory pathways of Sox9a.

Materials and methods

Zebrafish. Zebrafish TAB lines (hybrid from AB and Tubingen lines) were maintained under an ambient temperature of 27 °C with a timer-controlled light period of 14 h light and 10 h dark. All experiments were performed in accordance with the Animal Care and Use Committee guidelines of the Shanghai Ocean University.

Histological analysis and TUNEL staining. Fish were anesthetized in 0.1% tricaine (3-aminobenzoic acid ethyl-ester methanesulphonate salt; Sigma, Poole, UK) in filtered system water. Gonads were fixed with 4% paraformaldehyde, sectioned, and stained with hematoxylin and eosin (HE).²⁵ For TUNEL staining, paraffin-embedded sections were created following the manufacturer's protocol and subsequently stained in DAPI (Invitrogen Molecular Probes, Carlsbad, CA, USA) for 5 min, followed by two rinses in phosphate-buffered saline (PBS) for 10 min. After photography, the sections were counterstained with HE, and photographed.

In situ hybridization. Whole-mount *in situ* hybridization and histological *in situ* hybridization experiments were conducted as described previously.²⁵ Complementary DNAs corresponding to the target genes were used to generate riboprobes.

Immunohistochemistry and quantitative analysis. Immunohistochemistry was performed as described previously.²⁶ Antibodies used for the study include sox9a antibody (ab82578), anti-Erk1 + Erk2 antibody (ab54230), phosphorylated Erk1 + Erk2 (Phospho T202 + Y204) antibody (ab76165), and p53 antibody (ab77813). Fluorochrome-conjugated secondary antibodies, goat anti-rabbit Ig-FITC (ab6717), goat anti-mouse IgG-TR (ab6787), Dylight 594 rabbit anti-goat IgG (RAG5942), Dylight488 goat anti-mouse IgG (GAM4882), Dylight549, and goat anti-rabbit (GAR5492), were purchased from Abcam (Hong Kong) Ltd (Hong Kong) or Beijing CoWin Biotech Co., Ltd (Beijing, China). The sections were counterstained with Hoechst 33258 (Sigma) and then mounted with prolong antifade reagent (Invitrogen P7481).

To localize and quantify gene expression, color intensity of the immunostaining signals were quantified by using Adobe Photoshop 7.0 (Adobe Systems Inc., San Jose, CA, USA). The image was first converted as grayscale mode. The lasso tool palette was then used to draw a line around the edges of the cell. After opening the image-histogram window, the values for the selection were recorded as mean, S.D., median and pixels. The same procedure was repeated to collect background intensity. After subtracting the background signals, the remaining signal values represented the immunostaining intensity for the specific antibody in the selected cell. For each image, we collected histogram information from five cells and input the values in Excel spreadsheet. To perform comparison and data analyses we selected two parameters: the mean to represent the average gray value for the area inside the selection, and the pixel values to measure the image size.

RNA isolation and quantitative real-time PCR (RT-PCR). Total RNA was isolated using Trizol reagent (Invitrogen) and reverse transcribed to cDNA with Transcript II two-step RT-PCR supermix (Transgen Biotech, Beijing, China) in the presence of oligo (dT) 20 primer. Quantitative RT-PCR was carried out using 7500 Real-Time PCR System (Applied Biosystems, Foster City, CA, USA) and data analyses were performed as previously described.^{25,27} Oligonucleotide primers (listed in Supplementary Table 2) were synthesized by Shanghai Sangon Biological Engineering Technology and Service Co. Ltd (Shanghai, China).

Gonadal tissue culture. Basic gonadal tissue culture medium (GTCM) was based on the zebrafish testis and ovary growth medium in the previous reports.²³ L-15 (Leibovitz's L-15 medium, Gibco, Life Technologies, Carlsbad, CA, USA) was supplemented with 2 mM L-glutamine (Gibco), 50 U/ml penicillin and 50 µg/ml streptomycin (Gibco), 100 µg/ml kanamycin sulfate (Gibco), and 20% AmnioPAN complete medium (PAN Biotech GmbH, Aidenbach, Germany) with and without 10 IU/ml HCG (Sigma). After anesthesia with 0.1% tricaine, testes or ovary were removed from 2–3-month-old adult fish and sliced into 1.5 mm sections.³ The gonadal fragments were then plated on gelatin-coated Labtek dishes and incubated at 28 °C in air. After culture, the cells were fixed in 2% buffered paraformaldehyde for 2 h, and permeabilized with 0.2% PBT (0.2% Triton X-100 in PBS) for 10 min. The slides were ready for RNA *in situ* hybridization, HE staining, or immunostaining. Monoethanolate (U0126), 2-2-amino-3-methoxyphenyl (PD098), and cAMP (D0627) were purchased from Sigma and used at final concentrations of 20 µM, 10 µM, and 1 mM, respectively.

Conflict of Interest

The authors declare no conflict of interest.

Acknowledgements. We thank Qingyi Liang, Xinyi Wang, and others in the Yan Lab for their technical assistance and helpful discussions. We also thank two anonymous reviewers for their constructive critics to improve our manuscript. We gratefully acknowledge the support of Xin Yang, Xianyi Wang, Bolin Li, Jiale Li, Weidong Zhen, and Yingjie Pan. This work was supported in part by the international Cooperation Initiative Program of Shanghai Ocean University to JY (A0209-13-0808), the Innovation Program of Shanghai Municipal Education Commission to JY (13ZZ126), and Shanghai Universities First-class Disciplines Project of Fisheries. The funders had no role in the study design, data collection and analysis, decision to publish, or preparation of the manuscript.

1. Wilhelm D, Palmer S, Koopman P. Sex determination and gonadal development in mammals. *Physiol Rev* 2007; **87**: 1–28.
2. De Felici M. Origin, migration, and proliferation of human primordial germ cells. In: Santis GCD (ed) *Oogenesis*, Vol. XII. Springer: London, 2013, pp 19–37.

3. McClelland K, Bowles J, Koopman P. Male sex determination: insights into molecular mechanisms. *Asian J Androl* 2012; **14**: 164–171.
4. Kobayashi Y, Nagahama Y, Nakamura M. Diversity and plasticity of sex determination and differentiation in fishes. *Sex Dev* 2013; **7**: 115–125.
5. Uchida D, Yamashita M, Kitano T, Iguchi T. Oocyte apoptosis during the transition from ovary-like tissue to testes during sex differentiation of juvenile zebrafish. *J Exp Biol* 2002; **205**(Pt 6): 711–718.
6. Maack G, Segner H. Morphological development of the gonads in zebrafish. *J Fish Biol* 2003; **62**: 895–906.
7. Nobrega RH, Greebe CD, van de Kant H, Bogerd J, de Franca LR, Schulz RW. Spermatogonial stem cell niche and spermatogonial stem cell transplantation in zebrafish. *PLoS One* 2010; **5**: 9.
8. Guigon CJ, Coudouel N, Mazaud-Guittot S, Forest MG, Magre S. Follicular cells acquire sertoli cell characteristics after oocyte loss. *Endocrinology* 2005; **146**: 2992–3004.
9. Wang XG, Orban L. Anti-Mullerian hormone and 11 beta-hydroxylase show reciprocal expression to that of aromatase in the transforming gonad of zebrafish males. *Dev Dyn* 2007; **236**: 1329–1338.
10. Albrecht KH, Eicher EM. Evidence that Sry is expressed in pre-Sertoli cells and Sertoli and granulosa cells have a common precursor. *Dev Biol* 2001; **240**: 92–107.
11. Jameson SA, Natarajan A, Cool J, De Falco T, Maatouk DM, Mork L *et al*. Temporal transcriptional profiling of somatic and germ cells reveals biased lineage priming of sexual fate in the fetal mouse gonad. *PLoS Genet* 2012; **8**: e1002575.
12. Moore FL, Jaruzelska J, Dorfman DM, Reijo-Pera RA. Identification of a novel gene, DZIP (DAZ-interacting protein), that encodes a protein that interacts with DAZ (deleted in azoospermia) and is expressed in embryonic stem cells and germ cells. *Genomics* 2004; **83**: 834–843.
13. Nilsson EE, Schindler R, Savenkova MI, Skinner MK. Inhibitory actions of Anti-Mullerian Hormone (AMH) on ovarian primordial follicle assembly. *PLoS One* 2011; **6**: e20087.
14. Anderson JL, Rodriguez Mari A, Braasch I, Amores A, Hohenlohe P, Batzel P *et al*. Multiple sex-associated regions and a putative sex chromosome in zebrafish revealed by RAD mapping and population genomics. *PLoS One* 2012; **7**: e40701.
15. Bradley KM, Breyer JP, Melville DB, Broman KW, Knapik EW, Smith JR. An SNP-based linkage map for zebrafish reveals sex determination loci. *G3 (Bethesda)* 2011; **1**: 3–9.
16. Liew WC, Bartfai R, Lim Z, Sreenivasan R, Siegfried KR, Orban L. Polygenic sex determination system in zebrafish. *PLoS One* 2012; **7**: e34397.
17. Rodriguez-Mari A, Yan YL, Bremiller RA, Wilson C, Canestro C, Postlethwait JH. Characterization and expression pattern of zebrafish Anti-Mullerian hormone (Amh) relative to *sox9a*, *sox9b*, and *cyp19a1a*, during gonad development. *Gene Expr Patterns* 2005; **5**: 655–667.
18. Rodriguez-Mari A, Postlethwait JH. The role of Fanconi anemia/BRCA genes in zebrafish sex determination. *Methods Cell Biol* 2011; **105**: 461–490.
19. Nakamura S, Watakabe I, Nishimura T, Toyoda A, Taniguchi Y, Tanaka M. Analysis of medaka *sox9* orthologue reveals a conserved role in germ cell maintenance. *PLoS One* 2012; **7**: e29982.
20. Lasala C, Scheingart HF, Arouche N, Bedecarras P, Grinspon RP, Picard JY *et al*. SOX9 and SF1 are involved in cyclic AMP-mediated upregulation of anti-Mullerian gene expression in the testicular prepubertal Sertoli cell line SMAT1. *Am J Physiol Endocrinol Metab* 2011; **301**: E539–E547.
21. Taieb J, Grynberg M, Pierre A, Arouche N, Massart P, Belville C *et al*. FSH and its second messenger cAMP stimulate the transcription of human anti-Mullerian hormone in cultured granulosa cells. *Mol Endocrinol* 2011; **25**: 645–655.
22. Rodriguez-Mari A, Wilson C, Titus TA, Canestro C, BreMiller RA, Yan YL *et al*. Roles of *brca2* (*fancd1*) in oocyte nuclear architecture, gametogenesis, gonad tumors, and genome stability in zebrafish. *PLoS Genet* 2011; **7**: e1001357.
23. Kobayashi A, Chang H, Chaboissier MC, Schedl A, Behringer RR. Sox9 in testis determination. *Ann N Y Acad Sci* 2005; **1061**: 9–17.
24. von Hofsten J, Olsson PE. Zebrafish sex determination and differentiation: involvement of FTZ-F1 genes. *Reprod Biol Endocrinol* 2005; **3**: 63.
25. Wang X, He H, Tang W, Zhang XA, Hua X, Yan J. Two origins of blastemal progenitors define blastemal regeneration of zebrafish lower jaw. *PLoS One* 2012; **7**: e45380.
26. Yan J, Yang Y, Zhang H, King C, Kan HM, Cai Y *et al*. Menin interacts with IQGAP1 to enhance intercellular adhesion of beta-cells. *Oncogene* 2009; **28**: 973–982.
27. Yan J, Chen YX, Desmond A, Silva A, Yang Y, Wang H *et al*. *Cdx4* and menin co-regulate *hoxa9* expression in hematopoietic cells. *PLoS One* 2006; **1**: e47.



Cell Death and Disease is an open-access journal published by Nature Publishing Group. This work is licensed under a Creative Commons Attribution-NonCommercial-NoDerivs 3.0 Unported License. To view a copy of this license, visit <http://creativecommons.org/licenses/by-nc-nd/3.0/>

Supplementary Information accompanies this paper on Cell Death and Disease website (<http://www.nature.com/cddis>)